POWER AND ENERGY FUTURE

Open Access
Research Article

The Potential of Building Internal Thermal Mass to Create Energy Flexibility

Yihan Chen, Wenxin Huang, Priya Vishnu, Simeng Li, and Wentao Wu

***Abstract*—Solar resource provides clean and renewable energy for buildings, but solar radiation causes inherent problems to building space cooling. Internal thermal mass can be used to absorb and release solar heat gain at a time lag to shave peak cooling load and to create energy flexibility. This study recasts Li's analytical thermal mass model to include discrete time-varied solar heat gains as an additional boundary condition. The recast model is incorporated into the radiant time series method to quantify the reduction in the peak and total cooling load. The model is also used to assess how the characteristics of the thermal mass affect the cooling load. Results show that the presence of the internal thermal mass decreases the peak cooling load from 1930.2 ± 216.1 to 1339.7 ± 192.6 W in a single zone in Auckland. The combination of nighttime natural ventilation and daytime solar radiation absorption can reach a maximum cooling load reduction by 44.1%. Greater cooling load reduction is achieved by using the internal thermal mass in the West coast of South Island in New Zealand. The maximum peak and total cooling load reduction reaches 11.8 and 95.3 Wh·m^{-2} per day, respectively, in South West Cape.**

***Index Terms*—Energy efficiency, solar radiation, space cooling, natural ventilation, building modelling.**

ABBREVIATION

RTS	radiant time series

I. INTRODUCTION

Solar resource provides clean and renewable energy for buildings and is a key driver of decarbonisation [1], [2]. However, solar radiation is intermittent [3] and also causes inherent problems to building space cooling [4]. In summer, solar radiation is a major component of the cooling load [5], [6]. Excess solar gains in summer increase peak cooling load which is detrimental to building energy flexibility. Energy flexibility is defined as "the ability to manage its demand and generation according to local climate conditions, user needs, and grid requirements" [7]. To enhance energy flexibility, peak cooling load can be shaved by using the building thermal mass to absorb and release the solar heat gain at a time lag [8], [9].

Thermal mass can be incorporated into either external envelopes or internal floor slabs to manage solar heat gains [8]. An external thermal mass of 2 MJ·K^{-1} sheds peak cooling load by 53.4 W·m^{-2} and an internal thermal mass of the same amount decreases peak power by 13.2 W·m^{-2} [8]. Nighttime cooling can improve the performance of internal thermal mass to achieve a maximum net free cooling energy storage of 6.11 kWh·m^{-2}·a^{-1} in a climate with large daily temperature ranges [10], [11]. The combination of lightweight external construction with internal thermal mass shows better performance on shaving cooling load [12]. The internal thermal mass releases 43 ± 2.2 Wh·m^{-2} of the heat at night but absorbs only 15 ± 4.2 Wh·m^{-2} of the heat during the day. The low efficiency in heat absorption might be attributed to the incapability of the existing thermal mass model to address the solar irradiation on the thermal mass surface.

Previous studies infer optimum thickness and thermal properties for the internal thermal mass materials [10], [12]. The existing work emphasizes on energy analysis without exploring the mechanism of material thickness and thermal properties affecting the efficiency of the thermal mass to absorb and release heat [13]. Understanding these mechanisms requires information on the temperature distribution within the thermal mass. However, obtaining internal temperature data in real buildings is difficult. Concrete slab as a popular thermal mass material, after construction, is difficult probed with existing low-cost temperature sensors [14]. Mathematical modelling of heat transfer in thermal mass is a feasible solution. Finite element or finite difference method to solve heat conduction L can provide detailed temperature profiles in thermal mass [15], [16]. However, these numerical methods are time-consuming when they are integrated into building load calculation software or whole-building energy simulation program. As the whole-building energy simulation program is run at a time step of 10 min, but numerical methods require a time step of few seconds to ensure numerical stability. Reduced-order

Manuscript received 20 November, 2025; accepted 30 March, 2026. *(Yihan Chen and Wenxin Huang contributed equally to this work. Corresponding author: Wentao Wu, e-mail: w.wu2@massey.ac.nz)*

Y. Chen, W. Huang, P. Vishnu, S. Li and W. Wu are with the School of Built Environment, Massey University, Auckland, New Zealand.

Color versions of one or more of the figures in this paper are available online at https://doi.org/10.26599/PEF.2026.9650006.

Digital Object Identifier 10.26599/PEF.2026.9650006

© The author(s) 2026. Published by Tsinghua University Press.
This is an open access article under the Creative Commons Attribution 4.0 International License (http://creativecommons.org/licenses/by/4.0/).

models have a limitation of either short prediction time span of 12 h like RC or assumption of sinusoidal boundary conditions [17].

To overcome the shortcomings of the existing mathematical models for internal thermal mass, Wu et al. developed a one-dimensional analytical model suitable for discrete hourly varied indoor air temperatures [10]. The one-dimensional model was integrated into simple heat balance equations to describe daytime air conditioning and nighttime ventilation. Wu's model has a limitation in assuming constant convection heat transfer coefficients over the internal thermal mass [10]. Li et al. expanded the one-dimensional model to deal with more realistic boundary conditions including both time-varied indoor air temperatures and convection heat transfer coefficients [12]. The internal thermal mass model is further incorporated into RTS method to quantify various types of cooling loads [18]. The RTS method is a simplified cooling load calculation approach, which converts radiant heat gains into time-delayed cooling loads using time series factors. It accounts for the effect of heat being absorbed by building surfaces and subsequently released to the indoor air over time. Compared to the detailed heat balance method, RTS provides a computationally efficient way to estimate cooling loads while capturing the temporal effects of heat storage and release. The RTS method is used to link the dynamic response of internal thermal mass to cooling load formation, enabling the evaluation of its potential in shifting peak cooling demand. However, Li's model considers only convection heat transfer between the internal thermal mass and the room air, and the solar heat gain on the surface of internal thermal mass is still missing [12]. Addressing this missing boundary condition is essential for accurately evaluating the role of internal thermal mass under solar radiation.

This study aims to evaluate the performance of internal thermal mass in shifting solar heat gain to enhance building energy flexibility. Specifically, Li's analytical model [12] is recast to include discrete time-varied solar heat gains as an additional boundary condition. New chamber experiments have been conducted to understand the influence of the indoor air temperature measurement and convection heat transfer coefficient estimation on the accuracy of the model. The new model is incorporated into the RTS method to quantify the potential of internal thermal mass to shift peak cooling load and part heating load. The study also examines how thermal mass material properties and boundary conditions influence the cooling performance predicted by the model. Finally, the potential of applying internal thermal mass to improve energy flexibility is explored in 32 New Zealand cities.

II. MATERIALS AND METHODS

A. Laboratory Experiments for Model Validation

The climate chamber in the work of Li et al. [12] was used to collect air and thermal mass temperature histories for model validation. The chamber had a floor area of 8.98 m^2 covered with black sand pavers as the internal thermal mass. The paver had a thermal mass of 4.01 $MJ \cdot K^{-1}$. A heat pump (MODEL MPPD27H, Midea®) was used to heat up the internal thermal mass via convection.

Three thermal couples of type-12K were used to measure air temperatures near the supply outlet of the heat pump, in the middle of the chamber, and near the return inlet of the heat pump. Three thermal couples were attached to the top and bottom surface, respectively, of the internal thermal mass to measure the temperature profiles. The measurements were carried out for 48 days. In the first 24 h, the heat pump was off to allow the thermal mass and the chamber air temperature to equilibrate toward the same initial temperature. In the beginning of the second 24 h, the heat pump was set to 30 °C and run on and off according to the setpoint temperature. After three on–off cycles, the heat pump was switched off until the chamber air and the thermal mass reaching heat balance. Temperature data were recorded into a computer at a time interval of 1 min. The convection heat transfer coefficient was estimated according to the similar experiments presented in the work of Li et al. [12]. Convection heat transfer coefficients of 2–4 $W \cdot m^{-2} \cdot K^{-1}$ were used to test the model sensitivity to boundary conditions.

B. Incorporating Solar Heat Gain into Li's Model

The evolution of the temperature profile (T) in the internal thermal mass with time (t) can be obtained by solving the one-dimensional heat conduction equation:

$$C\frac{\partial T}{\partial t} = \lambda\frac{\partial^2 T}{\partial y^2} \tag{1}$$

$$\begin{aligned} &y = L:\ -\lambda\frac{\partial T}{\partial y} = h(T - T_r) - q_{sol} \\ &y = 0:\ \frac{\partial T}{\partial y} = 0 \\ &t = 0:\ T = T_r(0), q_{sol} = 0 \end{aligned} \tag{2}$$

where C is the thermal mass or heat capacity ($J \cdot K^{-1} \cdot m^{-3}$), λ is the thermal conductivity ($W \cdot K^{-1} \cdot m^{-1}$), y is the distance measured from the bottom of the internal thermal mass (m), L is the thickness of the thermal mass (m), h is the convection heat transfer coefficient ($W \cdot m^{-2} \cdot K^{-1}$), T_r is the room air temperature (K), and q_{sol} is the time-variant solar heat gain absorbed by the internal mass ($W \cdot m^{-2}$). The negative sign of q_{sol} denotes solar radiation heat flux transferring from surface to interior. To avoid the tedious process of applying Fourier transform, an indoor sol-air temperature T_{sol} is defined to recast Li's model:

$$T_{sol} = T_r + \frac{q_{sol}}{h} \tag{3}$$

The temperature field in the thermal mass can be described by Eq. (4).

清華大學出版社 Tsinghua University Press | SciOpen

$$T = T_r(0)\left\{\sum_{n=1}^{\infty}\varphi_n\left[\cos(\beta_n\eta) - \cos\beta_n\,(Bi - Bi(0))\,\frac{\eta^2-1}{2}\right] + \frac{\eta^2-1}{2}Bi\,\theta_{sol}\right\} + T_r(0)$$

$$\eta = \frac{y}{L}$$

$$Bi = \frac{hL}{\lambda}$$

$$\theta_{sol} = \frac{T_{sol} - T_r(0)}{T_r(0)}$$

$$\varphi_n = \frac{1}{W4_{m,n}}\left\{\sum_{j=0}^{m-1} e^{-\sum_{i=j}^{j-1} W2_{i+1,n}(\tau_{i+1}-\tau_i)}\, G_{j,n} + G_{m,n}\right\}$$

$$\tau = \frac{\lambda t}{CL^2}$$

$$G_{j,n} = A_{j+1,n}\left\{\frac{W1_{j+1,n}}{W2_{j+1,n}}\left[1 - e^{-W2_{j+1,n}(\tau_{i+1}-\tau_i)}\right] - W3_{j+1,n}e^{-W2_{j+1,n}(\tau_{i+1}-\tau_i)}\right\} \quad (4)$$

$T_r(0)$ is the initial temperature of room air. This model requires the initial temperature of the internal thermal mass equals the initial value of T_r. ϕ_n and G_n describes the time terms of the solution to the heat equations and their initial values are zero. β_n is the nth root of a transcendental equation with $Bi(0)$ as a coefficient. Bi is the Biot number that describes the internal conductive resistance of thermal mass to external convective resistance. θ_{sol} is the dimensionless indoor sol-air temperature. τ is the dimensionless time that characterises how fast heat can spread through the internal thermal mass. Coefficients A and W are time dependent and functions of the indoor sol-air temperature and the convection heat transfer coefficient. The detailed equations for A and W can be found in the work of Li et al. [12].

C. Incorporating the New Internal Thermal Mass Model into the RTS Method

The RTS method does not consider zone air heat balance [18]. Cooling load (Q_{cl}) is determined based on a constant setpoint temperature. The first step of the method is determining incident solar radiation and calculating heat gains (Fig. 1). Heat gains are split into radiative and convective portions. The radiative portion is converted into radiative cooling load using RTS. The summation of the convective portion and the corresponding radiative cooling load provides the individual type of cooling load, including the conductive cooling load through exterior walls and roofs, the conductive cooling load through windows, the cooling load due to solar heat gain through windows, the cooling load due to internal heat gains, and the cooling load due to infiltration. 60% of the solar heat gain is assumed to be incident on the internal thermal mass with a surface area of A and solar heat gain intensity is q_{sol}. This assumption ensures that the solar heat gain transmitted through the windows is primarily incident on the floor. It is not uniformly distributed across all the interior surfaces. The internal thermal mass model is incorporated into the heat balance equations [12], [19] through the convection heat transfer between the zone air (T_r) and the internal thermal mass surface ($T(L,t)$). The heat balance equations describe the heat balance of a zone with an ideal air conditioning system to maintain a constant setpoint temperature during the day and with natural ventilation during the night. The estimation of the natural ventilation rate and the convection heat transfer coefficient can be found in the work of Li et al. [12].

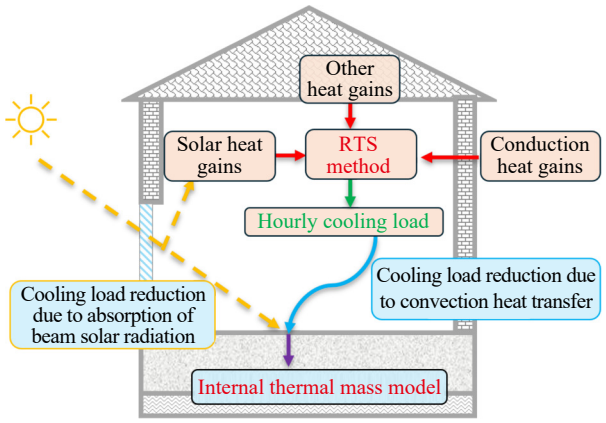

Fig. 1. The coupling between the RTS Method and the internal thermal mass model.

D. Energy Flexibility

The single zone in the work of Li et al. is used for case studies [12], [18]. The external wall is was designated to face the south in New Zealand. Different wall and roof assemblies listed in Tables 16, 17, and 18 in Chapter 18 of ASHRAE Handbook 2021 [20] are used for sensitivity test of the internal thermal mass to shave solar heat gains in the zone with light-, medium-, and heavyweight constructions. A combination of 830 external constructions is used to test the sensitivity. The conduction transfer function coefficients and U-values of the external constructions are provided in ASHRAE Handbook. The absorptivity of walls and roofs is specified as 0.55. Concrete floor slab is used as the internal thermal mass with a value of 21.6 $MJ \cdot K^{-1}$. The thermal conductivity of concrete is taken as 1 $W \cdot m^{-1} \cdot K^{-1}$, which lies within the typical range reported for normal-weight concrete and is close to the value used in the work of Li et al. Infiltration and internal heat gains are not considered in this study. The setpoint temperature for cooling is 23.3 °C between 8 am and 8 pm. The natural ventilation is enabled during the rest of the day. The 24-h outdoor air temperatures are generated using the 0.4% design dry-bulb temperature, which reflects the extreme cooling condition used in load calculations, together with the daily temperature range of the hottest month.

Energy flexibility has been assessed in 32 New Zealand

cities with the design day information given by ASHRAE [21]. Key performance indicators including power peak shedding and energy reduction are utilised [8]. Energy flexibility has been shown to be related to the timing of cooling season events [22]. The hottest month is selected for energy flexibility calculations in summer. Power peak shedding represents the difference in the peak cooling load at a specific time of a day. Energy reduction determines the mitigation of the total cooling load. The cooling loads from 8 am to 8 pm are summed to calculate the energy reduction [8]. The above key performance indicators are used to assess the energy flexibility of a building with active cooling. For buildings without air conditioning, thermal peak shedding can be defined to assess the thermal resilience [8]. The thermal peak shedding evaluates the reduction in the peak temperature in a 24-h naturally ventilated zone with the internal thermal mass relative to a base case without the internal thermal mass. The transitional season, April, is selected for the calculation of the thermal peak shedding.

III. RESULTS AND DISCUSSION

A. Model Validation

The recast thermal mass model (Eq. (4)) requires the input of the zone sol-air temperature and the convection heat transfer coefficient. The convection heat transfer coefficient is about 3 $W \cdot m^{-2} \cdot K^{-1}$ estimated in the work of Li et al. [12]. The sensitivity of the recast model to the input of air temperature is shown in Fig. 2. The air temperatures are monitored near the supply air (red), in the middle of the chamber (orange), and near the return air (yellow). The air temperature profiles show the stratification in the chamber. The predicted surface temperatures (dashed lines) using the air temperature monitored in the middle of the chamber show a better agreement with the measured values (solid lines with solid circles). The maximum relative difference between the measured and predicted surface temperatures is 2.4 and −2.0 °C, respectively, for the top and the bottom surface. The maximum deviation occurs after the heat pump stops completely at the 2.08×10^4 s. The surface temperatures predicted using the air temperature measured in the middle of the chamber are used for the following analysis.

When the heat pump is turned on for 5.15×10^3 s (the first cycle), the measured top surface temperature increases from 20.9 to 25.0 °C (Fig. 2(a)). The predicted top surface temperature increases to 24.4 °C. When the setpoint temperature is reached, the heat pump is switched off for 240 s (the first cycle). During this period, the measured top surface temperature continues to increase to 25.0 °C, at a lower rate. The predicted top surface temperature shows a similar trend and reaches a similar value of 24.5 °C. In the second and third on–off cycle, a similar trend occurs for the measured and predicted top surface temperatures. After the heat pump is completely stopped, the air temperature monitored in the middle of the chamber drops to 26.2 °C after 240 s. In this period, the measured top surface temperature drops to 26.4 °C but the predicted top surface temperature reaches 27.5 °C. The predicted top surface temperature drops at a lower rate than the measurement and maintains 1.1 °C higher than the measurement. The deviation might be due to the difficulty in the estimation of the convection heat transfer coefficient in the natural convection process driven by the small temperature difference.

The measured and predicted bottom surface temperatures show a similar trend in the 3 on–off cycles. A noticeable difference is that the measured bottom surface temperature drops slightly during heat pump off period. But the predicted bottom surface temperature continues to rise during the off period. After the heat pump is completely stopped, the measured bottom surface temperature swiftly drops to the same temperature of 26.9 °C as the chamber air temperature after 1.69×10^4 s. However, the predicted bottom surface slowly decreases to 26.7 °C and results in a deviation of −1.5 °C.

The convection heat transfer coefficient varies during the

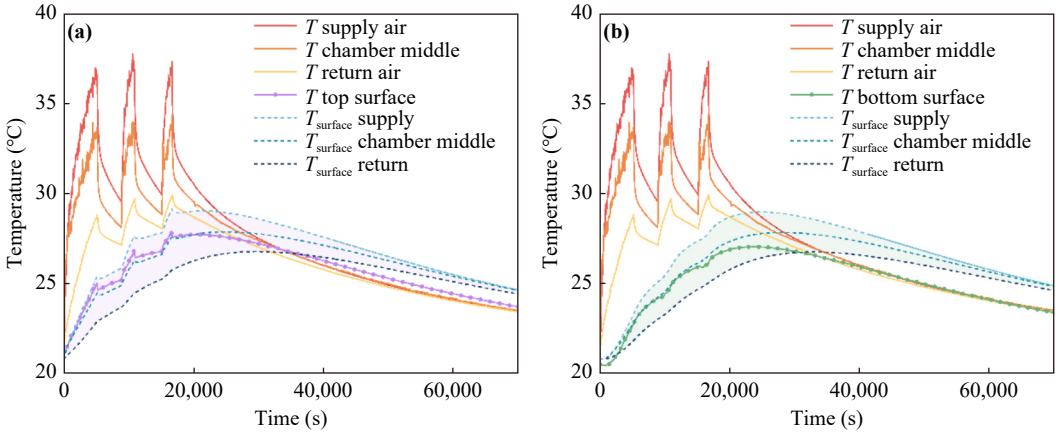

Fig. 2. Comparison of time–temperature profiles obtained from the chamber experiment and the model with air temperatures (solid lines) measured at three locations in the chamber. Solid lines with solid circles represent top (purple) and bottom (green) surface temperatures of the internal thermal mass. Dashed lines represent the corresponding surface temperatures calculated with the three air temperatures, respectively.

measurement. A constant value is used for the entire measurement period for simplicity. The convection heat transfer coefficient of 3 $W \cdot m^{-2} \cdot K^{-1}$ shows the best agreement between the measurement and the model during the on–off cycles. The maximum deviation occurs after the heat pump is completely stopped and reaches −1.0 and −1.6 °C for the top and the bottom surface, respectively. A small convection heat transfer coefficient of 2 $W \cdot m^{-2} \cdot K^{-1}$ cannot reproduce the trend of fast and slow rate of temperature rise during the on and off period. Similar to Fig. 2, the predicted bottom surface temperature exceeds the predicted top surface temperature by 0.3 °C after 3.71×10^4 s. However, the measured bottom surface temperature did not exceed the measured top surface temperature. The results from the internal thermal mass model are consistent with the assumptions of the convection heat transfer on the top surface and the adiabatic bottom surface. The zone air temperature drops below the top surface temperature, then the top surface temperature stops ascending. When the top surface temperature declines below the bottom surface temperature, the bottom surface temperature starts to decrease. In the experiments, the bottom surface temperature starts to decline after the heat pump is switched off. It indicates heat loss through the ground despite of thorough insulation in the experiment. Another factor contributing to the deviation between the experiment and the model is the initial temperature difference of 2.7 °C between the chamber air (20.5 °C) and the bottom surface (23.2 °C) (Fig. 3(b)).

B. Energy Analysis

Fig. 4 shows the potential of the internal thermal mass to reduce the peak cooling load in a single zone in Auckland. Red boxes represent the cooling load without the presence of the internal thermal mass. Blue boxes represent the cooling load reduction with the internal thermal mass by considering only nighttime cooling. Green boxes represent the cooling load reduction by nighttime cooling of the internal thermal mass and daytime absorption of solar radiation. The distribution in each box represents the cooling load variation due to different configurations of the external envelopes. Without the internal thermal mass, the peak cooling load is 1930.2 ± 216.1 W. The standard deviation illustrates the variation in the peak cooling load between the light- and heavyweight external constructions. By nighttime cooling of the internal thermal mass, the peak cooling load decreases to 1909.3 ± 207.8 W due to the convective heat transfer between the cooler surface of the internal thermal mass and the warmer indoor air. By absorbing beam solar radiation, the peak cooling load further decreases to 1339.7 ± 192.6 W. The average power peak shedding is 590.5 W that is comparable to the predicted maximum power peak shedding of about 400 W in the work of Yoon and Wu [8]. At 8 am, the cooling load for the single zone with the internal thermal mass is 149.6 ± 133.3 W that is 17.9% higher than 126.9 ± 145.4 W without the internal thermal mass. It indicates that the heat is released from the internal thermal mass into the air at night. The performance of the internal thermal mass to reduce the peak cooling load is achieved by nighttime cooling and daytime solar radiation absorption. Only nighttime cooling can reduce the peak cooling load by only 1.09% in the Auckland climate. The combination of nighttime cooling and daytime solar radiation absorption can reach a maximum cooling load reduction by 44.1%, considering the optimum configuration of the internal thermal mass and the external envelope. This does not mean that the internal thermal mass is more efficient to absorb the solar radiation. The function of the internal thermal mass to reduce cooling load is activated by the indoor air temperature difference between the day and the night. Therefore, the use of nighttime cooling is indispensable.

In transitional seasons, the internal thermal mass has a potential to reduce the overheating risk in unconditioned spaces. Fig. 5 shows the variation of indoor air temperatures in a single zone with 24-h natural ventilation in April in Auck-

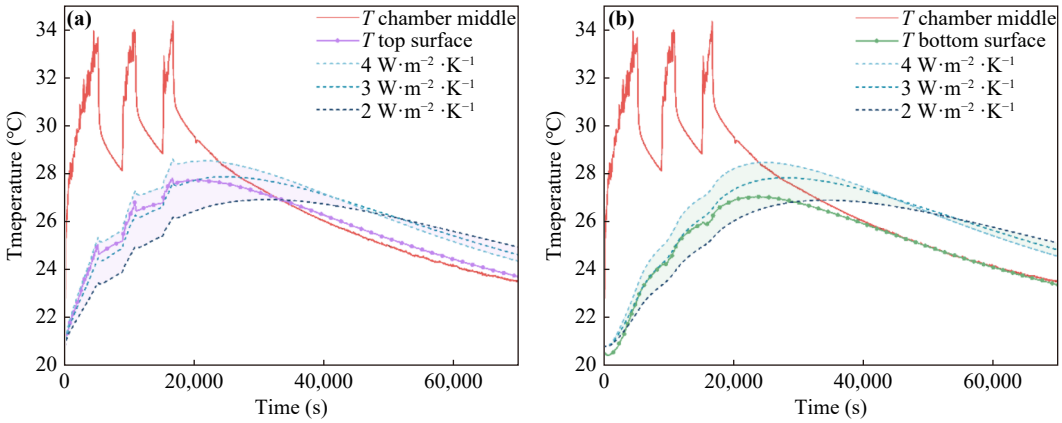

Fig. 3. Comparison of time-temperature profiles obtained from the chamber experiment and the model with three estimated convection heat transfer coefficients. The red line represents the air temperature measured in the middle of the chamber. Solid lines with solid circles represent top (purple) and bottom (green) surface temperatures of the internal thermal mass. The dashed lines represent the predicted top (a) and bottom (b) surface temperatures corresponding to 3 heat transfer coefficients: blue, light purple, and light green for 4, 3, and 2 $W \cdot m^{-2} \cdot K^{-1}$, respectively.

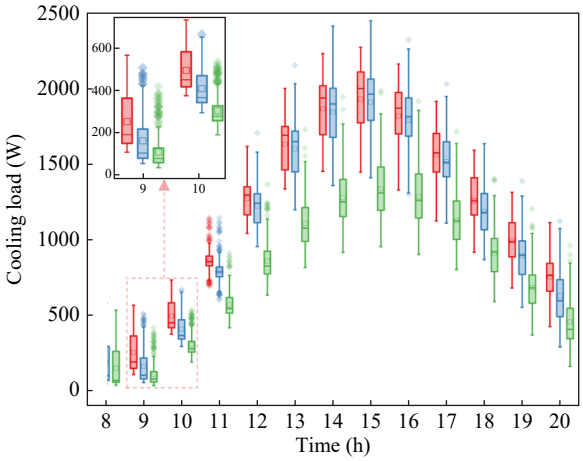

Fig. 4. Cooling load reduction using internal thermal mass in a single zone with different external construction configurations in February (summer) in Auckland. Red boxes represent the baseline case without thermal mass. Blue boxes represent the reduction calculated by Li's model. Green boxes represent the reduction calculated by the new model in this study.

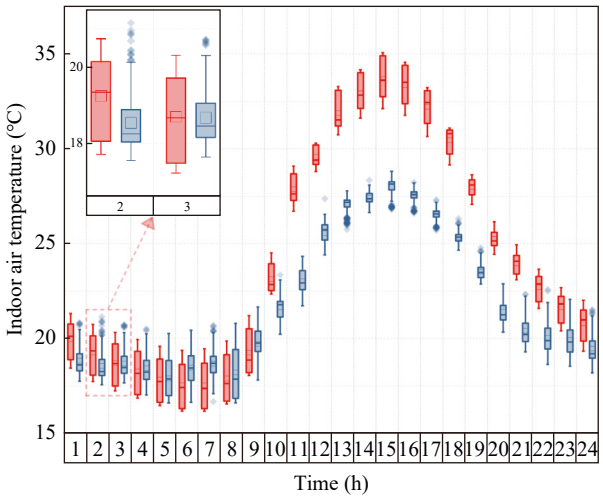

Fig. 5. Variation of indoor air temperature without (red boxes) and with (blue boxes) internal thermal mass in a single zone with different external construction configurations in April (fall) in Auckland. The single zone is assumed 24-hnatural ventilation.

land. When the indoor air temperature exceeds 28 °C in naturally ventilated spaces, the space is considered to be overheated. Without the internal thermal mass, the indoor air temperature in the single zone reaches 29.6 ± 0.5 °C at 12 pm. The indoor air temperature reaches the peak value of 33.7 ± 1.0 °C at 3 pm. After 8 pm, the indoor air temperature drops below 28 °C. Only natural ventilation is not adequate to mitigate the 8 overheating hours. The presence of the internal thermal mass maintains the indoor air temperatures below 28.0 ± 0.4 °C. The maximum air temperature reduction is about 6 °C that is comparable to the maximum air temperature reduction of 6 °C by using the internal thermal mass and natural ventilation in the work of Yoon and Wu [8]. The presence of the internal thermal mass also limits the indoor air temperature fluctuations. Without the internal thermal mass, the indoor air temperature varies between 32.1 and 35.1 °C at 3 pm depending on the external configurations. The internal thermal mass reduces the variation by 0.921 °C. The indoor air temperature drops to 17.5 ± 1.1 °C at 7 am due to the nighttime natural ventilation. Adding internal thermal mass maintains the indoor air temperature above 18 °C (18.7 ± 0.7 °C) and avoids overcooling.

C. Energy Flexibility

The potential of the internal thermal mass to create energy flexibility is explored for 32 New Zealand cities (Fig. 6). The bubble color represents the peak cooling load reduction, and the bubble size represents the total cooling load reduction between 8 am and 8 pm. Reductions in overall and peak cooling loads are generally greater on the west coast of the south Island and in the central part of the island at higher latitudes as a result of the application of thermal mass, while reductions are overall smaller on the north coast. The minimum peak cooling load reduction is 3.65 $Wh \cdot m^{-2}$ for the single zone in Gisborne, and the minimum total cooling load reduction is 33.6 $Wh \cdot m^{-2}$ per day. In the largest city, Auckland, the peak cooling load reduction is 6.19 $Wh \cdot m^{-2}$, and the total cooling load reduction is 51.2 $Wh \cdot m^{-2}$ per day. Further to the south in the Northern Island, the peak cooling load reduction reaches to 8.25 $Wh \cdot m^{-2}$ in the capital city, Wellington. The total cooling load reduction reaches 64.5 $Wh \cdot m^{-2}$ per day and increases by 26.0% compared to Auckland. The minimum peak cooling load reduction is 5.19 $Wh \cdot m^{-2}$ in the South Island. The minimum total cooling load reduction is 42.0 $Wh \cdot m^{-2}$ per day that is smaller than Gisborne. The maximum peak cooling load reduction reaches 11.8 $Wh \cdot m^{-2}$ in South West Cape. The total cooling load reduction in Invercargill is 95.3 $Wh \cdot m^{-2}$ per day, that is 1.86 times the reduction in Auckland.

IV. CONCLUSIONS

This study assesses the potential of the internal thermal mass to create energy flexibility by absorbing solar heat gain. Li's analytical thermal mass model is recast to include discrete time-varied solar heat gains as an additional boundary condition. The recast model is incorporated into the radiant time series method to quantify the reduction in the peak and total cooling load. Based on the improved model and the experimental validation, the following conclusions are drawn:

(1) The presence of the internal thermal mass decreases the peak cooling load from 1930.2 ± 216.1 to 1339.7 ± 192.6 W in a single zone in Auckland. The combination of nighttime natural ventilation and daytime solar radiation absorption can reach a maximum cooling load reduction by 44.1%, considering the optimum configuration of the internal thermal mass and the external envelope.

(2) The internal thermal mass can regulate the indoor air

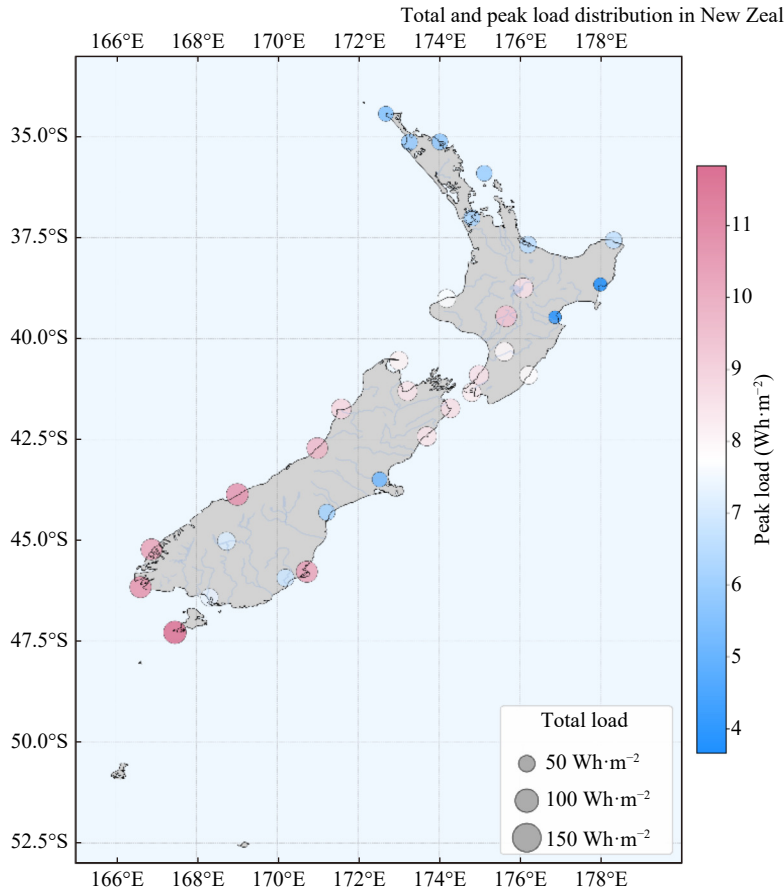

City	Total load (Wh·m^{-2})	Peak load (Wh·m^{-2})
Auckland	51.2	6.2
Cape Campbell	67.8	8.7
Cape Reinga	42.8	5.5
Castlepoint	61.5	7.9
Christchurch	42.0	5.2
Dunedin	56.8	6.8
Farewell Spit	64.2	8.1
Gisborne	33.6	3.7
Haast	89.2	10.8
Hicks Bay	53.3	6.6
Hokitika	81.6	9.8
Invercargill	57.6	7.3
Kaikoura	68.6	8.5
Kaitaia	49.1	5.8
Mokohinau	46.6	5.9
Napier	30.9	3.8
Nelson	70.4	8.5
New Plymouth	61.8	7.7
Plamerston North	66.3	8.0
Paraparaumu	71.4	8.6
Pururua	48.6	5.8
Puysegur Point	84.8	10.8
Queenstown	60.8	7.1
Secretary Island	83.3	10.3
South West Cape	95.3	11.8
Taiaroa Head	84.2	10.4
Taupo	72.2	8.6
Tauranga	54.2	6.5
Timaru	50.6	6.1
Waiouru	82.7	9.5
Wellington	64.5	8.2
Westport	73.9	8.9

Fig. 6. Cooling load reduction using the internal thermal mass from 8 am to 8 pm in summer in different New Zealand climates.

temperatures below 28.0 ± 0.4 °C in transitional seasons in Auckland. The maximum indoor air temperature reduction is about 6.9 °C that helps to reduce the overheating risk.

(3) More cooling load reduction is achieved on the west coast of the South Island and in the central region of New Zealand. The minimum peak cooling load reduction is 3.65 Wh·m^{-2} for the single zone in Gisborne, and the minimum total cooling load reduction is 33.6 Wh·m^{-2} per day. The maximum peak cooling load reduction reaches 11.8 Wh·m^{-2} in South West Cape. The total cooling load reduction in Invercargill is 95.3 Wh·m^{-2} per day.

The limitation of this study is that the RTS method can only determine cooling load. Future work will focus on the integration of the internal thermal mass model into whole-building energy simulation program. This would enable a more comprehensive evaluation of the internal thermal mass performance under realistic conditions. Further investigation into the interaction between internal thermal mass and whole-building simulation may also provide additional insights into energy flexibility.

Declaration of Competing Interest

The authors declare that they have no known competing financial interests or personal relationships that could have appeared to influence the work reported in this paper.

Funding

This work is carried out without the support of any funding agency.

AI Usage Statement

During the preparation of this manuscript, the authors used AI-assisted tools for language polishing only. The authors have reviewed and edited the content and take full responsibility for the final version of the manuscript.

References

[1] M. Sheikholeslami, Z. Khalili, F. Salehi, and L. Momayez, "Simulation of sustainable solar thermal storage system involving photovoltaic panel equipped with nanofluid-based splitter considering self-cleaning coating," *Sustain. Cities Soc.*, vol. 119, pp. 106100, Feb. 2025.

[2] A. Valencia, M. U. Hossain, and N. B. Chang, "Building energy retrofit simulation for exploring decarbonization pathways in a community-scale food-energy-water-waste nexus," *Sustain. Cities Soc.*, vol. 87, no. 4, pp. 104173, Dec. 2022.

[3] Y. N. Chen, L. Feng, I. B. Mansir, M. Taghavi, and K. Sharma, "A new coupled energy system consisting of fuel cell, solar thermal collector, and organic Rankine cycle; Generation and storing of electrical energy," *Sustain. Cities Soc.*, vol. 81, pp. 103824, Jun. 2022.

[4] I. Csáky and F. Kalmár, "Effects of solar radiation asymmetry on buildings' cooling energy needs," *J. Build. Phys.*, vol. 40, no. 1, pp. 35–54, Jul. 2016.

[5] D. A. Chwieduk, "Solar energy impact on space heating and cooling needs in moderate climate," *IOP Conf. Ser.: Mater. Sci. Eng.*, vol. 415, pp. 012008, Aug. 2018.

[6] A. H. A. Mohammed, M. A. Hamid, and O. Kaynakli, "Solar radiation and energy efficiency: Analyzing the impact on cooling and heating in different climatic regions", in *Proceedings of the 11th Global Conference on Global Warming (GCGW 2023)*, 2023.

[7] S. Ø. Jensen, A. Marszal-Pomianowska, R. Lollini, W. Pasut, A. Knotzer, P. Engelmann, A. Stafford, and G. Reynders, "IEA EBC Annex 67 Energy Flexible Buildings," *Energy Build.*, vol. 155, pp. 25–34, Nov. 2017.

[8] N. Yoon and W. T. Wu, "Short-term thermal resilience and building energy flexibility using thermal mass and controlled natural ventilation," *Energy Build.*, vol. 320, pp. 114547, Oct. 2024.

[9] J. Fadejev, R. Simson, J. Kurnitski, and M. Bomberg, "Thermal mass and energy recovery utilization for peak load reduction," *Energy Procedia*, vol. 132, pp. 39–44, Oct. 2017.

[10] W. T. Wu, J. Benner, and Z. W. Luo, "Developing analytical model for nighttime cooling of internal thermal mass," *Appl. Therm. Eng.*, vol. 220, pp. 119798, Feb. 2023.

[11] B. Chenari, J. Dias Carrilho, and M. Gameiro da Silva, "Towards sustainable, energy-efficient and healthy ventilation strategies in buildings: a review," *Renew. Sustain. Energy Rev.*, vol. 59, pp. 1426–1447, Jun. 2016.

[12] M. T. Li, X. Shen, W. T. Wu, K. Cetin, F. Mcintyre, L. Z. Wang, L. X. Ding, D. Bishop, L. Bellamy, and M. Liu, "Cooling demand reduction with nighttime natural ventilation to cool internal thermal mass under harmonic design-day weather conditions," *Appl. Energy*, vol. 379, pp. 124947, Feb. 2025.

[13] C. Gao, Y. Liu, R. Q. You, and H. W. Li, "Theoretical and numerical study on thermal insulation performance of thermal barrier coatings," *Energies*, vol. 15, no. 19, pp. 6880, Sep. 2022.

[14] T. Y. Wang, D. Li, J. J. Zhou, and J. Zhang, "Temperature monitoring of mass concrete structure using wireless sensing system," *Struct. Control Health Monit.*, vol. 2025, no. 1, pp. 7847074, Apr. 2025.

[15] C. X. Shi, R. P. Niu, and C. T. Wu, "The thermal-mass-redistributed finite element method combined with the Houbolt method for 2D transient heat conduction problems," *Int. J. Comput. Methods*, vol. 22, no. 3, pp. 2342009, Apr. 2025.

[16] M. S. Arif, K. Abodayeh, and Y. Nawaz, "An application of the finite element method for heat and mass transfer of boundary layer flow using variable thermal conductivity and mass diffusivity," *J. Math.*, vol. 2022, no. 1, pp. 7929161, Sep. 2022.

[17] S. Fresca, L. Dede', and A. Manzoni, "A comprehensive deep learning-based approach to reduced order modeling of nonlinear time-dependent parametrized PDEs," *J. Sci. Comput.*, vol. 87, no. 2, pp. 61, Apr. 2021.

[18] F. C. McQuiston, J. D. Parker, J. D. Spitler, and H. Taherian, *Heating, Ventilating, and Air Conditioning: Analysis and Design*, Hoboken, NJ: John Wiley & Sons, 2023.

[19] L. Yang and Y. Li, "Cooling load reduction by using thermal mass and night ventilation", *Energy Build.*, vol. 40, no. 11, pp. 2052–2058, 2008.

[20] ASHRAE, *ASHRAE Handbook—Fundamentals*. ASHRAE, 2021.

[21] ASHRAE, "ASHRAE climatic design conditions," 2025. [Online]. Available: https://ashrae-meteo.info/v3.0/.

[22] J. Vivian, U. Chiodarelli, G. Emmi, and A. Zarrella, "A sensitivity analysis on the heating and cooling energy flexibility of residential buildings," *Sustain. Cities Soc.*, vol. 52, pp. 101815, Jan. 2020.



Yihan Chen received the M.S. degree in Environmental Design and Engineering from University College London (UCL), U.K. She is currently pursuing the Ph.D. degree with the School of Built Environment, Massey University, New Zealand. Her research focuses on building energy performance and passive technologies.



Wenxin Huang received the M.S. degree in health, wellbeing, and sustainable buildings from University College London (UCL), U.K. She is currently pursuing the Ph.D. degree in civil engineering at Colorado School of Mines, U.S.A. Her research focuses on building resilience and energy efficiency.



Priya Vishnu received the Ph.D. degree in Mechanical Engineering from the University of Canterbury, New Zealand. She is currently a Lecturer in Building Services and a Doctoral Supervisor with the School of Built Environment, Massey University, Auckland, New Zealand. Her research focuses on building energy consumption, seismic damping systems, and sustainability in the built environment.



Simeng Li is currently a Lecturer with the School of Built Environment, Massey University, New Zealand. Her research interests include building energy efficiency.



Wentao Wu is an Associate Professor at Massey Univeristy, New Zealand. He was a tenure-track Assistant Professor in the Department of Civil and Architectural Engineering at Tennessee State University (TSU). Prior to joining TSU, He worked as a postdoctoral researcher at Harvard University. He received his Ph.D. degree in engineering at Aarhus University (2012, Denmark). He worked in danish industry for a couple of years. Then he returned to academics and did his first postdoctoral research at ETH Zürich.